Curado-Carballada , Ch., Feixas, F. & Osuna, S. *Molecular Dynamics Simulations on Aspergillus niger Monoamine Oxidase: Conformational Dynamics and Inter-monomer Communication Essential for Its Efficient Catalysis*, 2019, 361 (11), 2718-2726.

DOI: 10.1002/adsc.201((will be filled in by the editorial staff))

Molecular Dynamics Simulations on *Aspergillus niger* Monoamine Oxidase: Conformational Dynamics and Inter-monomer Communication Essential for Its Efficient Catalysis

Christian Curado-Carballada [a], Ferran Feixas [a]*, and Sílvia Osuna [a,b]*

[a] Institut de Química Computacional i Catàlisi (IQCC) and Departament de Química, Carrer Maria Aurèlia Capmany 69, 17003 Girona, Catalonia, Spain
E-mail: ferran.feixas@udg.edu, silvia.osuna@udg.edu
[b] ICREA, Pg. Lluís Companys 23, 08010 Barcelona, Spain

Received: ((will be filled in by the editorial staff))

Supporting information for this article is available on the WWW under http://dx.doi.org/10.1002/adsc.201######.((Please delete if not appropriate))

Abstract. *Aspergillus niger* Monoamine Oxidase (MAO-N) is a homodimeric enzyme responsible for the oxidation of amines into the corresponding imine. Laboratory evolved variants of MAO-N in combination with a non-selective chemical reductant represents a powerful strategy for the deracemisation of chiral amine mixtures and, thus, is of interest for obtaining chiral amine building blocks. As we reported recently, MAO-N presents a rich conformational dynamics with a flexible ß-hairpin region that can adopt closed, partially closed and open states. Despite the ß-hairpin conformational dynamics is altered along the laboratory evolutionary pathway of MAO-N, the connection between the ß-hairpin conformational dynamics and how this affects active site catalysis still remains unclear. In this work, we use accelerated molecular dynamics to elucidate the potential interplay between the ß-hairpin conformational dynamics and catalytic activity in MAO-N wild type (WT) and its evolved D5 variant. Our study reveals a delicate communication between both MAO-N monomers that impacts the active site architecture, and thus its catalytic efficiency. In both MAO-N WT and the laboratory evolved D5 variant, the ß-hairpin conformation in one of the monomers affects the productive binding of the substrate in the active site of the other subunit. However, both MAO-N WT and D5 variants show a quite different behaviour due to the impact of distal mutations introduced experimentally with Directed Evolution on the conformational dynamics of the enzyme.

Keywords: Monoamine Oxidase; Conformational Dynamics; Biocatalysis; Inter-monomer Communication; Accelerated Molecular Dynamics

Introduction

During the last decades, the use of biocatalysts in pharmaceutical industry for obtaining chiral compounds has been expanded.[1] Approximately 50% of drugs contain at least one chiral amine building block, which are, indeed, hardly affordable by traditional chemical transformations.[2] In this context, many efforts have been devoted to engineer natural enzymes for obtaining enantiomerically pure amines suitable for its use at industrial scale.[2] A particularly relevant enzyme in this regard is Monoamine Oxidase from *Aspergillus niger* (MAO-N).[3] MAO-N is a dimeric flavoenzyme, *i.e.* Flavin Adenine Dinucleotide (FAD) dependent, responsible for the oxidation of amines into the corresponding imine by means of cofactor reduction (see Figure 1). The reaction takes place inside a hydrophobic cavity formed by the aromatic side chains of residues Trp430 and Phe466, which are responsible for stabilizing the amine substrate close to the isoalloxazine ring of the FAD. The interest for this enzyme mainly arises from its promising catalytic activity towards different amine substrates.[4] In 2003, Turner and co-workers developed a strategy for the deracemisation of chiral amine mixtures, utilizing MAO-N in combination with a non-selective chemical reductant, such as sodium borohydride.[4a] This fact broadened the application of MAO-N as biocatalyst for the production of enantiomerically pure amines. Notwithstanding, the wild-type (WT) enzyme was only active towards primary and some secondary amines, being the biosynthesis of pure tertiary amines still hampered.[4a] In this regard, many efforts were put to achieve a smart library of variants that improved the catalytic activity

of MAO-N as well as broadened its substrate scope towards bulkier amines.[4b, 4c] With this purpose, many Directed Evolution (DE) experiments were performed resulting in different MAO-N variants that presented different substrate scope for imine production.[4b, 4c] The active site mutation (N336S) identified in the first round of DE enhanced the k_{cat} approximately 50-fold towards alpha-methylbenzylamine (AMBA).[4d] Subsequent rounds of evolution increased the activity towards AMBA but also broadened the substrate scope for other substrates.[4e] From these studies we can highlight MAO-N D5, which was the first MAO-N variant able of catalysing the oxidation of different aromatic secondary amines with high conversions and enantioselectivities.[4b] Interestingly, the introduced mutations via DE were located not only at the active site (N336S), but also at distal positions (M348K, T384N, D385S) including a mutation at the substrate entrance channel (I246M), *i.e.* at the interface of the two monomers, (See Figure 1). These distal mutations key for evolving MAO-N towards higher activities for bulkier substrates were recently found to profoundly affect the conformational dynamics of the MAO-N enzyme.[5]

The view of enzymes seen as an ensemble of multiple conformations of importance for its function, promiscuity, and evolution has gained increasing attention during recent years.[6] Computational tools have shown to be extremely useful in unveiling the conformational dynamics of enzymes and in explaining its key role for recognizing and binding the substrate, releasing the product, and catalysis.[7] The ensemble of conformations other than the native state that enzymes can adopt in solution can be mapped in the so-called Free Energy Landscape (FEL), in which the most stable conformations and the energy barriers that separate them are represented. By introducing mutations, a redistribution of the relative stabilities of the existing enzyme conformations can be achieved, which might affect the enzyme activity. This is indeed the case of MAO-N, as shown by a recent study from our group.[5] By means of extensive Molecular Dynamics (MD) simulations we evaluated the conformational dynamics of MAO-N WT and its D5 variant. The reconstruction of the associated FEL revealed the existence of some hidden partially closed, and hidden open conformations not previously observed by means of X-ray crystallography or NMR studies. Interestingly, the relative stabilities of the closed, hidden partially closed, and hidden open states were dramatically different in WT and D5 as a result of the laboratory evolution. The introduced mutations via DE therefore induced a redistribution of the relative stabilities of the states to favour the closed conformation in D5. Our study also demonstrated that such distal mutations, challenging to be predicted by means of rational approaches, can be identified by careful inspection of the conformational dynamics of the enzyme through the developed Shortest Path Map (SPM).[5, 8]

Similarly to what has been observed in other unrelated enzymes,[9] our previous simulations indicated that the

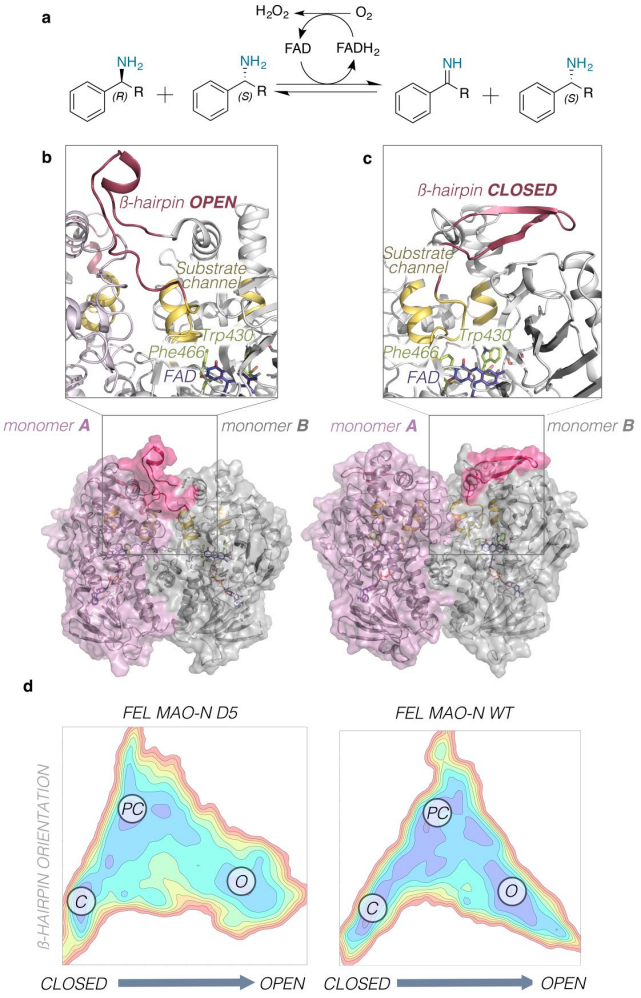

highly flexible ß-hairpin region of MAO-N modulates substrate access to the active site and its recognition. These simulations revealed the substrate binding pathway to the MAO-N WT and D5 active sites, however, detailed analysis of how the ß-hairpin

Figure 1. a) MAO-N general reaction scheme, b-c) Representation of the MAO-N homodimer (chain A in pink, chain B in grey) in the (b) hidden open state of the ß-hairpin of monomer B revealed by extensive Molecular Dynamics (MD) simulations performed in previous study,[5] and in the (c) closed (or X-ray like) conformation of the ß-hairpin B. An active site zoom at the open and closed states is represented, where the FAD cofactor is shown in purple, the hydrophobic cage residues Phe466 and Trp430 in green, the substrate channel in yellow, and ß-hairpin in pink. d) Previously computed conformational landscape for both MAO-N WT and D5 variant. The different conformational states are highlighted: closed (**C**), hidden partially closed (**PC**), and open (**O**).

conformation influences the active site pre-organization for efficient catalysis was not evaluated in detail in our previous study. Therefore, the connection between the ß-hairpin conformational dynamics and how this affects active site catalysis still

remains unclear. Interestingly, the analysis of the residues involved in the conformational exchange with our SPM tool[5] suggested that the conformation of the ß-hairpin of one of the monomers of the enzyme has an impact in the active site residues of the other subunit. This is in line with previous studies suggesting that the reaction only occurs in one of the monomers, being the other in charge of cofactor regeneration.[10] Interestingly, the binding of an inhibitor in a cavity located at the active site entrance of MAO-B was found to be enhanced after inhibitor binding at the active site of the enzyme, thus suggesting inter-monomer communication within the enzyme.[11] Such allosteric effects have also been identified in other unrelated enzymes.[12] In this study, we aim to investigate the potential interplay between the ß-hairpin conformational dynamics, inter-monomer communication between subunits, and active site pre-organization in MAO-N WT and its evolved D5 variant. Our substrate-bound MD simulations reveal that the ß-hairpin conformation dramatically impacts the active site structure of the other subunit of the enzyme, thus confirming that efficient catalysis in MAO-N is regulated by inter-monomer communication induced by ß-hairpin conformational dynamics.

Results and Discussion

As pointed out in the introduction, the interplay between the ß-hairpin conformational dynamics and how this affects the active site pre-organization for catalysis still remains unclear. To this end, we performed substrate-bound MD simulations of MAO-N considering different ß-hairpin conformations to explore the stability of the substrate in the active site pocket and whether catalytically productive poses are sampled in the different open/closed states. The interplay between ß-hairpin conformational dynamics and catalysis is first evaluated in the evolved variant MAO-N D5, and later on in MAO-N WT.

Interplay between ß-hairpin dynamics and catalysis in MAO-N D5

To further elucidate how the ß-hairpin conformation might affect catalysis in MAO-N D5 active site we used the enhanced sampling technique accelerated Molecular Dynamics (aMD) simulations[13] with alpha-methylbenzylamine (AMBA) as substrate bound in the active site. aMD allows a fast exploration of the accessible conformational states of the enzyme, which might play a role in substrate recognition and catalysis. Initial structures of MAO-N D5 corresponding to either closed or open conformations of the ß-hairpin in monomer B (and always maintaining the ß-hairpin of monomer A in the closed conformation) were taken from our previous study (see Figure 2).[5] To assess the connection between monomer B ß-hairpin conformational dynamics and monomer A catalysis, the substrate was docked in the active site cavity of the A subunit using Autodock Vina for open and closed states of monomer B ß-hairpin (Figure 2).x[14] We selected as starting point for our aMD simulations those binding poses of AMBA in which the aromatic ring interacts with both aromatic cage residues (in a T-shape conformation) and the isoalloxazine ring of the FAD cofactor via π-stacking with the amine group of AMBA pointing towards the nitrogen of the FAD. To elucidate the interplay between ß-hairpin conformation of monomer B and active site pre-organization for efficient catalysis of AMBA in A, we analysed the ß-hairpin conformational changes that take place in the presence of substrate. To this end, the conformations visited along these aMD simulations were projected on the previously reconstructed conformational landscape of MAO-N D5 that describes the possible ß-hairpin states of monomer B: closed (or X-ray like, **C** in Figure 1d), the hidden partially closed (**PC**), and hidden open state (**O**, see grey landscape in Figure 1d and 3a).[5] To distinguish those conformations visited along the aMD simulation presenting catalytically productive distances for amine oxidation, a colouring scheme was used: catalytic distances (*i.e.* AMBA(N) – FAD(N)) smaller than 3.5 Å were represented with green dots, whereas non-productive frames in teal (if the distances lie within 3.5-5 Å), light purple (5-6 Å), violet (6-7 Å), and dark purple (more than 7 Å), see coloured points in Fig 3a.

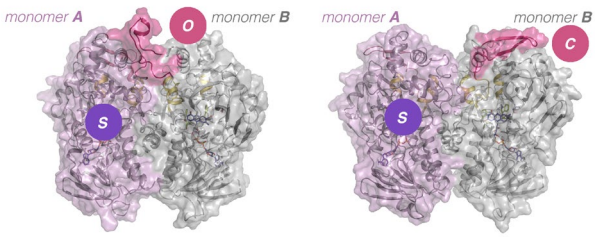

Figure 2. General scheme of the systems simulated with aMD. The substrates (purple spheres denoted with S) are always positioned in the active site of monomer A and two different conformations of MAO-N are considered: (left image) with the ß-hairpin of monomer B in the open (O) conformation and (right) with the ß-hairpin of monomer B in a closed (C) conformation.

Our study begins with the analysis of the simulations starting from the closed state of the ß-hairpin of monomer B (or X-ray like, **C** in Figure 1d), and positioning AMBA in the active site of monomer A which also displays a ß-hairpin in the closed state (see Figure 3a, green dots). The projection of one of the aMD replicas performed shows many catalytically competent productive poses for amine oxidation, which occur while the ß-hairpin of monomer B is maintained in the closed conformation (see accumulation of green dots in the vicinity of **C** state, Figure 3a). By counting the number of frames that display catalytic distances below the threshold value (*i.e.* 3.5 Å) we observe a 54.5% of catalytically

productive frames, with mean distances of 3.8 ± 0.9 Å (Figure 3a) indicating that the substrate remains in the active site during the whole simulation time. By careful analysis of the catalytically active frames

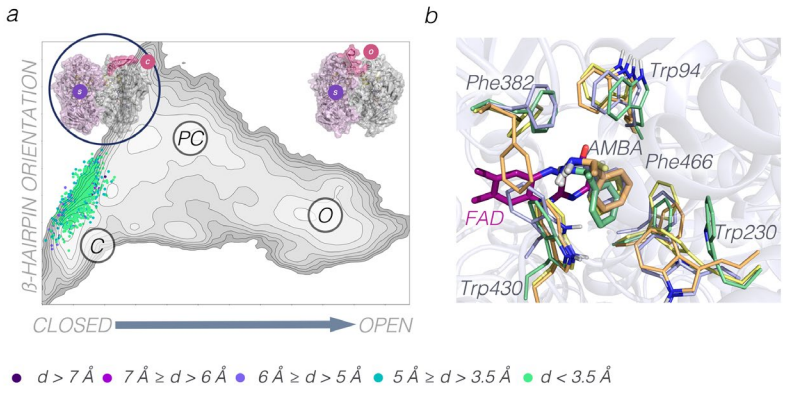

Figure 3. a) Projection of one of the aMD simulations starting from the closed state (**C**) of the ß-hairpin and positioning AMBA in the active site of monomer A on a previously computed conformational landscape of MAO-N D5 that differentiates among closed (**C**), partially closed (**PC**), and open (**O**) states of the ß-hairpin of monomer B. Each conformation sampled in the aMD simulation is represented with a dot coloured according to the value of the AMBA(N) – FAD(N) catalytic distance (d): catalytically productive frames are marked in green (d < 3.5 Å), whereas non-productive frames either in teal (3.5-5 Å), light purple (5-6 Å), violet (6-7 Å), or dark purple (d > 7 Å). b) Overlay of representative frames visited along the aMD simulation. Each frame is represented with a different colour (yellow, orange, blue, green), and FAD cofactor is shown in purple.

visited along the aMD simulations, we observe that the substrate is always interacting via π-stacking with the isoalloxazine ring of the FAD, and in a T-shape conformation with the residues forming the aromatic cage (*i.e.* Phe466 and Trp430) pointing the amine group of AMBA towards FAD(N) (see Figure 3c). The visual analysis of selected conformations confirms that AMBA is properly oriented for catalysis and also the active site residues remain stable along the simulation time (see Figure 3b). In particular, Trp94 and Phe382, which are responsible of keeping AMBA inside the aromatic cage, do not show significant conformational changes along the aMD trajectories. The introduced Asn336Ser mutation, which is found next to Trp430, provides extra stability and space to the aromatic cage allowing the proper orientation of AMBA. In the conformations where short catalytic distances are sampled, the aromatic ring of AMBA is always properly positioned in the aromatic cage for productive catalysis, thanks to the latter Asn336Ser mutation. These simulations thus confirm that productive amine oxidation in monomer A of D5 is achieved when the ß-hairpin in monomer B adopts a closed conformation.

A completely different picture is observed in the simulations in which AMBA is located in the active site of monomer A, but the ß-hairpin in monomer B is in a hidden open state (**O**, in Figure 4). When the ß-hairpin of monomer B stays in the open conformation catalytic distances are hardly sampled (see Figure 4a). In contrast to the closed conformation, the open state of the ß-hairpin favors the side chain rotation of residues Trp230, Leu245, and Phe382 located in the active site of monomer A that increases the size of the pocket leaving more space for AMBA to leave from the aromatic cage (see Figure 4b).

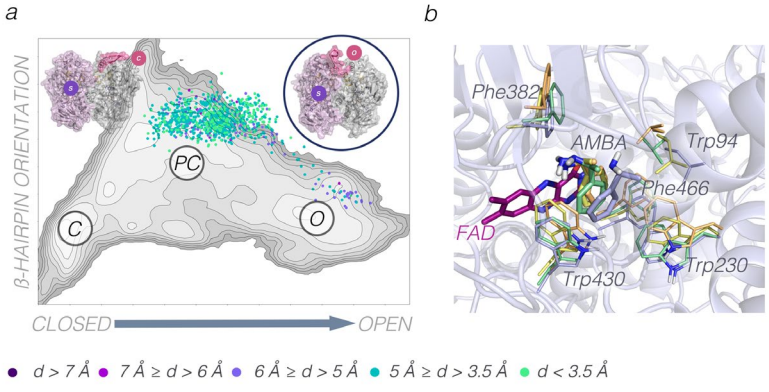

Figure 4. a) Projection of one of the aMD simulations starting from the openstate (**O**) of the ß-hairpin and positioning AMBA in the active site of monomer A on a previously computed conformational landscape of MAO-N D5 that differentiates among closed (**C**), partially closed (**PC**), and open (**O**) states of the ß-hairpin of monomer B. Each conformation sampled in the aMD simulation is represented with a dot coloured according to the value of the AMBA(N) –

FAD(N) catalytic distance (d): catalytically productive frames are marked in green (d < 3.5 Å), whereas non-productive frames either in teal (3.5-5 Å), light purple (5-6 Å), violet (6-7 Å), or dark purple (d > 7 Å). b) Overlay of representative frames visited along the aMD simulation. Each frame is represented with a different colour (yellow, orange, blue, green), and FAD cofactor is shown in purple.

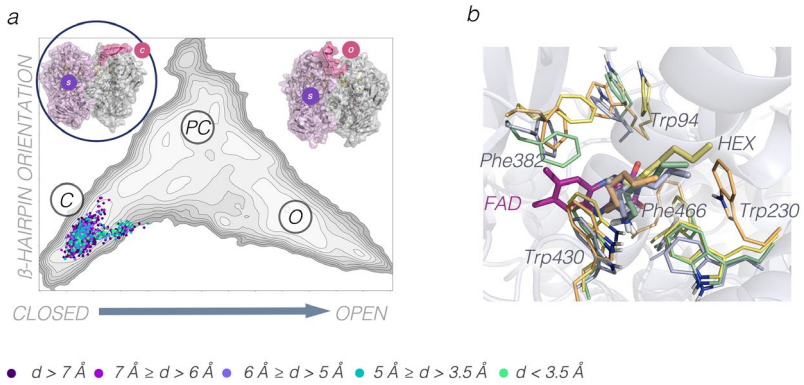

Figure 5. a) Projection of one of the aMD simulations starting from the closed state (**C**) of the ß-hairpin and positioning HEX in the active site of monomer A on a previously computed conformational landscape of MAO-N WT that differentiates among closed (**C**), partially closed (**PC**), and open (**O**) states of the ß-hairpin of monomer B. Each conformation sampled in the aMD simulation is represented with a dot coloured according to the value of the AMBA(N) – FAD(N) catalytic distance (d): catalytically productive frames are marked in green (d < 3.5 Å), whereas non-productive frames either in teal (3.5-5 Å), light purple (5-6 Å), violet (6-7 Å), or dark purple (d > 7 Å). b) Overlay of representative frames visited along the aMD simulation. Each frame is represented with a different colour (yellow, orange, blue, green), and FAD cofactor is shown in purple.

In our previous study, we found that the mutations introduced with DE stabilize the closed and partially closed states, thus being more accessible than the open state in D5.[5] Taken together with the new substrate-bound simulations performed here, the higher activity found experimentally for MAO-N D5 with AMBA is given by the increased stability of the closed and partially-closed states of the ß-hairpin, which are the catalytically productive ones.

Interestingly, there is a particular replica that after a few ns of aMD simulation the ß-hairpin of B rapidly escapes from the open state evolving towards hidden partially closed conformations (**PC** in Figure 4a), as it can be observed in Figure 4a (see accumulation of points near **PC**). After this transition of the ß-hairpin of monomer B, the side chains of Trp230, Leu245, and Phe382 residues in monomer A are reverted back to its original position. A remarkable feature of this simulation is that as soon as the ß-hairpin B adopts a partially closed conformation, catalytically productive distances are sampled in the active site of monomer A (see green dots accumulated on **PC** in Figure 4a). Due to the initial open conformations of the ß-hairpin, we observe a decrease in the amount of catalytically productive frames with respect to the other simulation that started from the closed state, representing a 21.7% with mean distances of 6.7 ± 0.8 Å. This simulation therefore demonstrates that the hidden open state in MAO-N-D5 plays no role in efficiently catalyzing AMBA oxidation.

Overall these simulations for MAO-N D5 indicate that the conformational dynamics of the ß-hairpin in one monomer of the enzyme influences the active site architecture and thus the catalytic efficiency of the other subunit. Our results also show that closed and partially closed conformations of the ß-hairpin are crucial for effective catalysis in monomer A of MAO-N D5, inducing a stabilization of catalytically active poses of AMBA for efficient amine oxidation.

Interplay between ß-hairpin dynamics and catalysis in MAO-N WT

The impact of the conformational dynamics of the ß-hairpin in monomer B on the catalytic activity of monomer A of MAO-N WT was assessed using hexylamine (HEX) as substrate, as it presents poor activity towards AMBA.[4d, 15] The same protocol used for D5 was followed to explore the catalytic efficiency of the open and closed conformational states of MAO-N WT. As shown below, our aMD simulations reveal significant differences between both D5 and WT.

We started analysing the aMD simulations that begin in the closed **C** state of the ß-hairpin in monomer B, and HEX positioned by molecular docking in the active site of the other monomer A (see Figure 5). In Figure 5a, the different conformations visited along the aMD simulation are projected on the conformational landscape of MAO-N WT. This landscape discriminates among closed, partially closed and open states of the ß-hairpin. As described above for the D5 variant, the colour of the dots indicates how catalytically competent the different conformations visited are for amine oxidation. Although the simulation starts with HEX properly positioned in the active site of monomer A, the amine mostly adopts catalytically unproductive conformations, resulting in a 3.8% of catalytically productive frames with a mean catalytic distance of 8.2 ± 2.7 Å (see Figure 5a). By

visually analysing different frames visited along the aMD trajectory, some side-chain rotations of residues Trp94, Trp230 and Phe382 are observed (see Figure 5b). Such side-chain conformational changes expand the size of the active site cavity, thus allowing the substrate to leave the aromatic cage.

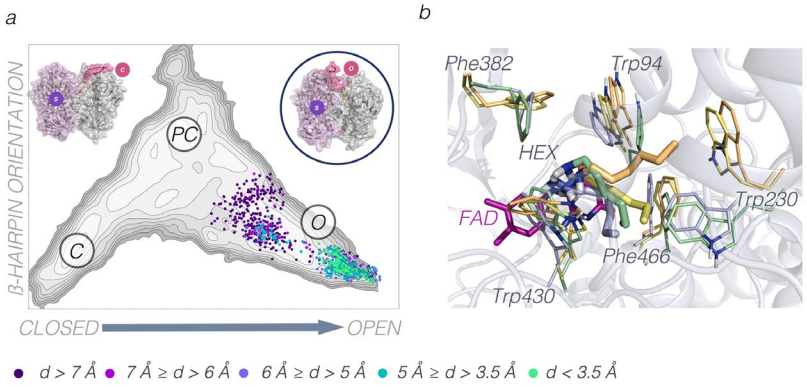

Figure 6. a) Projection of one of the aMD simulations starting from the open state (**O**) of the ß-hairpin and positioning HEX in the active site of monomer A on a previously computed conformational landscape of MAO-N WT that differentiates among closed (**C**), partially closed (**PC**), and open (**O**) states of the ß-hairpin of monomer B. Each conformation sampled in the aMD simulation is represented with a dot coloured according to the value of the AMBA(N) – FAD(N) catalytic distance (d): catalytically productive frames are marked in green (d < 3.5 Å), whereas non-productive frames either in teal (3.5-5 Å), light purple (5-6 Å), violet (6-7 Å), or dark purple (d > 7 Å). b) Overlay of representative frames visited along the aMD simulation. Each frame is represented with a different colour (yellow, orange, blue, green), and FAD cofactor is shown in purple.

This simulation suggests that the closed state of the ß-hairpin found to be key for activity in D5 is not as relevant for catalysis in WT. Interestingly, we found in our previous study that the closed conformation is significantly less stable in WT than in D5,[5] which combined with these new substrate-bound aMD simulations indicate that the least stable closed state of the MAO-N WT ß-hairpin is not relevant for catalysis.

The opposite behaviour is observed when starting the simulations from the open **O** state of the ß-hairpin in monomer B (see Figure 6). When the ß-hairpin remains in an open conformation, catalytically productive distances for amine oxidation are significantly sampled (see accumulation of green dots in **O** in Figure 6a). However, in the simulations that the system evolves towards partially-closed **PC** states, substrate unbinding takes also place. The analysis of the catalytic distances for HEX, establishing again a threshold of 3.5 Å to distinguish productive distances among non-productive ones, shows an 18.0% of catalytically active frames with a mean distance of 6.0 ± 2.3 Å. This number of catalytically productive frames is significantly higher and the mean distance lower (thus better for catalysis) than in the previous simulations that start with the ß-hairpin in the closed state. By carefully analysing the active site architecture at some representative conformations visited along the aMD simulation, we can observe that despite side-chain rotations of residues Trp230 and Phe382 taking place, HEX stays close to FAD sampling catalytically productive distances (see Figure 6b). This suggests that, in contrast to what we observe for D5, the role of the hydrophobic cage residues for properly positioning the substrate for catalysis is minor in WT enzyme. These simulations again reveal a delicate communication between both monomers of MAO-N, which is crucial for the enzyme activity. In contrast to D5, open states of the ß-hairpin in WT stabilize HEX substrate in catalytically productive conformations for amine oxidation. These results taken together with our previous study[5] indicate that open states of the ß-hairpin found to be highly stabilized as compared to the MAO-N D5 play a key role in HEX oxidation.

Conclusion

Although in a previous study we demonstrated the flexibility of a ß-hairpin region in MAO-N, how this flexibility affected the catalytic efficiency in each MAO-N active site remained elusive. The simulations based on the enhanced sampling technique aMD performed in this study have revealed a delicate communication between both MAO-N subunits that impacts the active site architecture, and thus its catalytic efficiency. In both MAO-N WT and the laboratory evolved D5 variant, the conformation of a flexible ß-hairpin in one of the monomers affects the catalytically productive binding of the substrate in the active site of the other subunit. However, both MAO-N WT and D5 variants behave quite differently due to the distal mutations introduced with Directed Evolution. In our previous study, we identified different relative stabilities for the closed, partially closed, and open states of MAO-N WT and MAO-N D5, which in this study we find it has a direct impact on the catalytic activity. In the evolved D5 variant, the closed conformation of the ß-hairpin found to be stabilized as compared to WT is the only one able of efficiently position the substrate in the active site of

the other monomer for productive catalysis. This is not the case for MAO-N WT for which the open conformation of the ß-hairpin is substantially more stable and essential for hexylamine oxidation in the other monomer. Therefore, we identify that the open state is the catalytically productive in MAO-N WT while the closed state is the catalytically productive in MAO-N D5. Our findings on the interplay between MAO-N ß-hairpin conformational dynamics and its connection to catalysis in the different monomeric units is crucial for the engineering of additional MAO-N variants, but also for unrelated homodimeric enzymes where similar conformational inter-monomer communication could also operate.

Experimental Section

Protein Preparation: Molecular Dynamics simulations (MD) were performed for MAO-N WT and MAO-N D5 in the presence of hexylamine (HEX) and alpha-methyl benzylamine (AMBA) substrates in the active site. As starting point for our MD simulations, we have selected representative structures from our previous study.[5] Initial structures of MAO-N WT and MAO-N D5 correspond to closed and open conformations of the ß-hairpin in monomer B (and always maintaining the ß-hairpin of monomer A in the closed conformation, see Figure 2). For MAO-N D5 MD simulations, AMBA was docked in the active site of monomer A of MAO-N-D5 using Autodock Vina.[14] We selected as starting point for our MD simulations those binding poses of AMBA in which the aromatic ring interacts with both aromatic cage (in a T-shape conformation) and the isoalloxazine ring of the FAD cofactor via π-stacking and the nitrogen of the amine group of AMBA is pointing towards the nitrogen of the isoalloxazine ring of the FAD cofactor establishing a hydrogen bond. For the MAO-N WT MD simulations, hexylamine substrate was docked in the active site of MAO-N WT using Autodock Vina. We selected as starting point for our MD simulations those binding poses of hexylamine in which the aliphatic chain is placed between the aromatic side chains of the aromatic cage residues Phe466 and Trp430 and the nitrogen of the amine group of hexylamine is pointing towards the nitrogen of the isoalloxazine ring of the FAD cofactor.

Molecular Dynamics Simulations details. Each system was immersed in a pre-equilibrated truncated cubic box of TIP3P water molecules with an internal offset distance of 10 Å, using the AMBER 16 LEAP module. All systems were neutralized with explicit counterions (Na^+ or Cl^-). All calculations were done using the ff99SBildn Amber force field[16] and TIP3P water model.[17] A two-stage geometry optimization approach was performed. First, a short minimization of the water molecules positions, with positional restraints on solute by a harmonic potential with a force constant of 500 kcal mol^{-1} $Å^{-2}$ was done. The second stage was an unrestrained minimization of all the atoms in the simulation cell. Then, the systems were gently heated using six 50 ps steps, incrementing the temperature 50 K each step (0-300 K) under constant-volume, periodic-boundary conditions and the particle-mesh Ewald approach[18] to introduce long-range electrostatic effects. For these steps, an 8 Å cutoff was applied to Lennard-Jones and electrostatic interactions. Bonds involving hydrogen were constrained with the SHAKE algorithm. Harmonic restraints of 10 kcal mol^{-1} were applied to the solute, and the Langevin equilibration scheme is used to control and equalize the temperature. The time step was kept at 2 fs during the heating stages, allowing potential inhomogeneities to self-adjust. Each system was then equilibrated for 2 ns with a 2 fs timestep at a constant pressure of 1 atm. After the systems were equilibrated in the NPT ensemble, MD simulations of 100 ns were performed under the NVT ensemble and periodic-boundary conditions using our Galatea cluster (composed by 178 GTX1080 GPUs). With Galatea, MAO-N simulations were performed at a speed of ca. 55 ns/day.

Substrate parameterization. The parameters for the FAD cofactor, HEX and AMBA substrates for the MD simulations were generated within the ANTECHAMBER module of AMBER 16 using the general AMBER force field (GAFF),[19] with partial charges set to fit the electrostatic potential generated at the HF/6-31G(d) level by the RESP model. The charges were calculated according to the Merz-Singh-Kollman scheme[20] using Gaussian 09.

Accelerated Molecular Dynamics Simulations. *Conformational dynamics*. Accelerated Molecular Dynamics simulations (aMD)[21] were used to explore the interaction between the substrate and the active site of MAO-N WT and MAO-N D5. We determined the acceleration parameters from the 100 ns unrestrained conventional MD simulations described above. For each system, five replicas of 200 ns of dual-boost accelerated Molecular Dynamics (aMD) simulations were carried out. In these simulations, we monitored the distance between the nitrogen of the amine group of the substrate and nitrogen of the FAD cofactor, i.e. AMBA(N) – FAD(N). In addition, aMD simulations were projected on to the Free Energy Landscape (FEL) of both MAO-N WT and MAO-N D5 to assess the conformational changes on the ß-hairpin of monomer B.

aMD enhances the conformational sampling of biomolecules, by adding a non-negative boost potential to the system when the system potential is lower than a reference energy:

$$V^*(r) = V(r), \qquad V(r) \geq E,$$
$$V^*(r) = V(r) + \Delta V(r), \; V(r) < E, \tag{1}$$

where $V(r)$ is the original potential, E is the reference energy, and $V^*(r)$ is the modified potential. In the simplest form, the boost potential, $\Delta V(r)$ is given by:

$$\Delta V(r) = \frac{(E - V(r))^2}{\alpha + E - V(r)}, \tag{2}$$

where α is the acceleration factor. As the acceleration factor α decreases, the energy surface is flattened more and biomolecular transitions between low-energy states are increased.

Here a total boost potential is applied to all atoms in the system in addition to a more aggressive dihedral boost, *i.e.*, (E_{dihed}, α_{dihed}; E_{total}, α_{total}), within the dual-boost aMD approach. The acceleration parameters used in this work, are the following:

$$E_{\text{dihed}} = V_{\text{dihed\_avg}} + 3.5 \times N_{\text{res}}, \alpha_{\text{dihed}} = 3.5 \times N_{\text{res}}/5;$$
$$E_{\text{total}} = V_{\text{total\_avg}} + 0.175 \times N_{\text{atoms}}, \alpha_{\text{total}} = 0.175 \times N_{\text{atoms}}, \tag{3}$$

where N_{res} is the number of protein residues, N_{atoms} is the total number of atoms, and $V_{\text{dihed\_avg}}$ and $V_{\text{total\_avg}}$ are the average dihedral and total potential energies calculated from 100 ns cMD simulations, respectively.

Free Energy Landscape of MAO-N WT and MAO-N D5: The Free Energy Landscapes (FEL) of MAO-N WT and MAO-N D5 were obtained from extensive MD simulations from our previous study.[5] In this previous study, 150 µs accumulated MD data were projected into a selected feature space, capturing the conformational change of the flexible β-hairpin. A feature set containing combinations of the C-alpha distances between β-hairpin loop residues 128-131, and the important β-sheet residues 353-356 as well as the

angle formed by the C-alpha atoms of residues 134 (monomer B), 240 (monomer A), and 360 (monomer B) were included. Afterwards, the time-lagged independent component analysis (TICA)[22] was used to generate a kinetically relevant space for each MAO-N WT and D5 system separately. The lag time selection of 10 ns was based on the description of 95% cumulative kinetic variance, including the smallest possible number of TICA dimensions. The generated FEL allows the discrimination between closed, partially closed, and open states of the β-hairpin in monomer B. AMD simulations were then projected on the FEL generated using this protocol to monitor conformational changes occurring on the ß-hairpin of monomer B in the presence of substrate in the other active site.

Acknowledgements

F.F. thanks the European Community for MSCA-IF-2014-EF-661160-MetAccembly grant, S. O. thanks the funding from the European Research Council (ERC) under the European Union's Horizon 2020 research and innovation programme (ERC-2015-StG-679001). We thank the Generalitat de Catalunya for grup emergent 2017 SGR-1707. We are grateful for the computer resources, technical expertise, and assistance provided by the Barcelona Supercomputing Center - Centro Nacional de Supercomputación.

References

[1] a) U. T. Bornscheuer, G. W. Huisman, R. J. Kazlauskas, S. Lutz, J. C. Moore, K. Robins, *Nature* **2012**, *485*, 185; b) M. D. Truppo, *ACS Med. Chem. Lett.* **2017**, *8*, 476-480.

[2] D. Ghislieri, N. J. Turner, *Top. Catal.* **2014**, *57*, 284-300.

[3] K. E. Atkin, R. Reiss, V. Koehler, K. R. Bailey, S. Hart, J. P. Turkenburg, N. J. Turner, A. M. Brzozowski, G. Grogan, *J. Mol. Biol.* **2008**, *384*, 1218-1231.

[4] a) R. Carr, M. Alexeeva, A. Enright, T. S. C. Eve, M. J. Dawson, N. J. Turner, *Angew. Chem. Int. Ed.* **2003**, *42*, 4807-4810; b) C. J. Dunsmore, R. Carr, T. Fleming, N. J. Turner, *J. Am. Chem. Soc.* **2006**, *128*, 2224-2225; c) D. Ghislieri, A. P. Green, M. Pontini, S. C. Willies, I. Rowles, A. Frank, G. Grogan, N. J. Turner, *J. Am. Chem. Soc.* **2013**, *135*, 10863-10869; d) M. Alexeeva, A. Enright, M. J. Dawson, M. Mahmoudian, N. J. Turner, *Angew. Chem. Int. Ed.* **2002**, *41*, 3177-3180; e) S. Herter, F. Medina, S. Wagschal, C. Benhaïm, F. Leipold, N. J. Turner, *Bioorganic Med. Chem* **2017**, *27*, 30391-30397; f) G. Li, P. Yao, R. Gong, J. Li, P. Liu, R. Lonsdale, Q. Wu, J. Lin, D. Zhu, M. T. Reetz, *Chem. Sci.* **2017**, *8*, 4093-4099; g) E. O'Reilly, C. Iglesias, D. Ghislieri, J. Hopwood, J. L. Galman, R. C. Lloyd, N. J. Turner, *Angew. Chem. Int. Ed.* **2014**, *53*, 2447-2450.

[5] C. Curado-Carballada, F. Feixas, J. Iglesias-Fernández, S. Osuna, *Angew. Chem. Int. Ed.* **2019**, *58*, 3097-3101.

[6] a) M. A. Maria-Solano, E. Serrano-Hervás, A. Romero-Rivera, J. Iglesias-Fernández, S. Osuna, *Chem. Commun.* **2018**, *54*, 6622-6634; b) N. Tokuriki, D. S. Tawfik, *Science* **2009**, *324*, 203-207.

[7] a) A. Romero-Rivera, M. Garcia-Borràs, S. Osuna, *Chem. Commun.* **2017**, *53*, 284-297; b) P. Dušan, K. Shina Caroline Lynn, *Curr. Opin. Struct. Biol.* **2018**, *52*, 50-57; c) D. J. Huggins, P. C. Biggin, M. A. Dämgen, J. W. Essex, S. A. Harris, R. H. Henchman, S. Khalid, A. Kuzmanic, C. A. Laughton, J. Michel, A. J. Mulholland, E. Rosta, M. S. P. Sansom, M. W. van der Kamp, *WIREs Comput. Mol. Sci.* **2018**, e1393; d) R. Vianello, C. Domene, J. Mavri, *Front. Neurosci.* **2016**, *10*, 327; e) A. Warshel, R. P. Bora, *J. Chem. Phys*. **2016**, *144*, 180901; f) R. E. Amaro, A. J. Mulholland *Nat. Rev. Chem.* **2018**, *2*, 0148; g) J. Åqvist, M. Kazemi, G. V. Isaksen, B. O. Brandsal, *Acc. Chem. Res.* **2017**, *50*, 199-207

[8] A. Romero-Rivera, M. Garcia-Borràs, S. Osuna, *ACS Catal.* **2017**, *7*, 8524-8532.

[9] a) A. Gora, J. Brezovsky, J. Damborsky, *Chem. Rev.* **2013**, *113*, 5871-5923; b) N. Kreß, J. M. Halder, L. R. Rapp, B. Hauer, *Curr. Opin. Chem. Biol.* **2018**, *47*, 109-116.

[10] V. J. DeRose, J. C. G. Woo, W. P. Hawe, B. M. Hoffman, R. B. Silverman, K. Yelekci, *Biochemistry* **1996**, *35*, 11085-11091.

[11] D. Bonivento, E. M. Milczek, G. R. McDonald, C. Binda, A. Holt, D. E. Edmondson, A. Mattevi, *J. Biol. Chem.* **2010**, *285*, 36849-36856.

[12] a) G. La Sala, S. Decherchi, M. De Vivo, W. Rocchia, *ACS Cent. Sci.* **2017**, *3*, 949-960; b) S. A. Wells, M. W. van der Kamp, J. D. McGeagh, A. J. Mulholland, *PLOS ONE* **2015**, *10*, e0133372.; c) M. D. Daily, H. Yu, G. N. Phillips, Q. Cui, *Top. Curr. Chem.* **2013**, *337*, 139-164; d) S. J. Wodak, E. Paci, N. V. Dokholyan, I. N. Berezovsky, A. Horovitz, J. Li, V. J. Hilser, I. Bahar, J. Karanicolas, G. Stock, P. Hamm, R. H. Stote, J. Eberhardt, Y. Chebaro, A. Dejaegere, M. Cecchini, J. P. Changeux, P. G. Bolhuis, J. Vreede, P. Faccioli, S. Orioli, R. Ravasio, L. Yan, C. Brito, M. Wyart, P. Gkeka, I. Rivalta, G. Palermo, J. A. McCammon, J. Panecka-Hofman, R. C. Wade, A. Di Pizio, M. Y. Niv, R. Nussinov, C. J. Tsai, H. Jang, D. Padhorny, D. Kozakov, T. McLeish, *Cell* **2019**, *27*, 566-578.

[13] a) D. Hamelberg, J. Mongan, J. A. McCammon, J. Chem. Phys. 2004, 120, 11919-11929; b) Y. Miao, F. Feixas, C. Eun, J. A. McCammon, *J. Comput. Chem.* **2015**, *36*, 1536-1549.

[14] O. Trott, A. J. Olson, *J. Comp. Chem.* **2010**, *31*, 455-461.

[15] B. Schilling, K. Lerch, Biochim. Biophys. *Acta, Gen. Subj.* **1995**, *1243*, 529-537.

[16] K. Lindorff-Larsen, S. Piana, K. Palmo, P. Maragakis, J. L. Klepeis, R. O. Dror, D. E. Shaw, *Proteins: Struct., Funct., Bioinf.* **2010**, *78*, 1950-1958.

[17] W. L. Jorgensen, J. Chandrasekhar, J. D. Madura, R. W. Impey, M. L. Klein, *J. Chem. Phys.* **1983**, *79*, 926-935.

[18] T. Darden, D. York, L. Pedersen, *J. Chem. Phys.* **1993**, *98*, 10089-10092.

[19] J. Wang, R. M. Wolf, J. W. Caldwell, P. A. Kollman, D. A. Case, *J. Comput. Chem.* **2004**, *25*, 1157-1174.

[20] B. H. Besler, K. M. Merz, P. A. Kollman, *J. Comp. Chem.* **1990**, *11*, 431-439.

[21] D. Hamelberg, J. Mongan, J. A. McCammon, *J. Chem. Phys.* **2004**, *120*, 11919-11929.

[22] G. Pérez-Hernández, F. Paul, T. Giorgino, G. De Fabritiis, F. Noé, *J. Chem. Phys.* **2013**, *139*, 015102.

UPDATE

Molecular Dynamics Simulations on *Aspergillus niger* Monoamine Oxidase: Conformational Dynamics and Inter-monomer Communication Essential for Its Efficient Catalysis

Adv. Synth. Catal. **Year**, *Volume*, Page – Page

Christian Curado-Carballada, Ferran Feixas,* Sílvia Osuna*

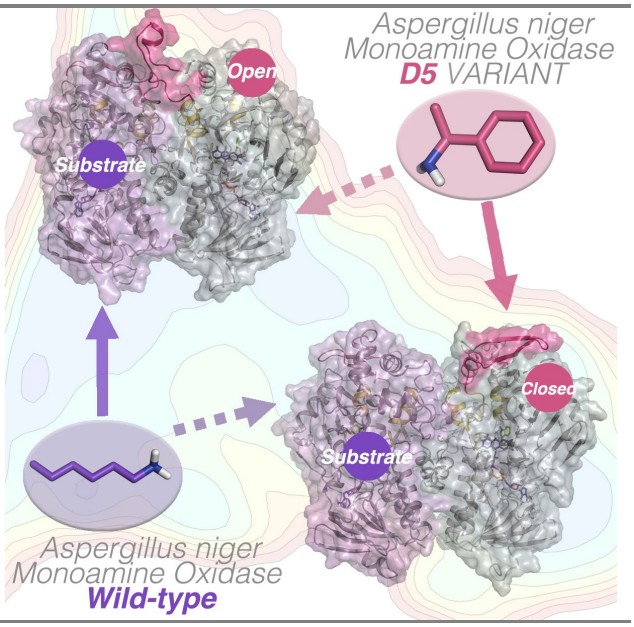

on